ORIGINAL RESEARCH ARTICLE

WILEY | *Journal of* Cellular Physiology

Inflammatory cytokines associated with cancer growth induce mitochondria and cytoskeleton alterations in cardiomyocytes

Maria Buoncervello[1]* | Sonia Maccari[2]* | Barbara Ascione[3] | Lucrezia Gambardella[3] |
Matteo Marconi[3] | Massimo Spada[4] | Daniele Macchia[4] | Tonino Stati[2] |
Mario Patrizio[2] | Walter Malorni[3,5] | Paola Matarrese[3] | Giuseppe Marano[2]† |
Lucia Gabriele[6]†

[1]Research Coordination and Support Service, Istituto Superiore di Sanità, Rome, Italy

[2]Center for Gender-Specific Medicine, Istituto Superiore di Sanità, Rome, Italy

[3]Center for Gender-Specific Medicine, Oncology Unit, Istituto Superiore di Sanità, Rome, Italy

[4]National Centre of Animal Research and Welfare, Istituto Superiore di Sanità, Rome, Italy

[5]Department of Biology, University of Tor Vergata, Rome, Italy

[6]Department of Oncology and Molecular Medicine, Istituto Superiore di Sanità, Rome, Italy

Correspondence
Paola Matarrese, Center for Gender-Specific Medicine, Oncology Unit, Istituto Superiore di Sanità, Rome, Italy
Email: paola.matarrese@iss.it

Abstract

Cardiac dysfunction is often observed in patients with cancer also representing a serious problem limiting chemotherapeutic intervention and even patient survival. In view of the recently established role of the immune system in the control of cancer growth, the present work has been undertaken to investigate the effects of a panel of the most important inflammatory cytokines on the integrity and function of mitochondria, as well as of the cytoskeleton, two key elements in the functioning of cardiomyocytes. Either mitochondria features or actomyosin cytoskeleton organization of in vitro-cultured cardiomyocytes treated with different inflammatory cytokines were analyzed. In addition, to investigate the interplay between tumor growth and cardiac function in an in vivo system, immunocompetent female mice were inoculated with cancer cells and treated with the chemotherapeutic drug doxorubicin at a dosing schedule able to suppress tumor growth without inducing cardiac alterations. Analyses carried out in cardiomyocytes treated with the inflammatory cytokines, such as tumor necrosis factor α (TNF-α), interferon γ (IFN-γ), interleukin 6 (IL-6), IL-8, and IL-1β revealed severe phenotypic changes, for example, of contractile cytoskeletal elements, mitochondrial membrane potential, mitochondrial reactive oxygen species production and mitochondria network organization. Accordingly, in immunocompetent mice, the tumor growth was accompanied by increased levels of the inflammatory cytokines TNF-α, IFN-γ, IL-6, and IL-8, either in serum or in the heart tissue, together with a significant reduction of ventricular systolic function. The alterations of mitochondria and of microfilament

----

system of cardiomyocytes, due to the systemic inflammation associated with cancer growth, could be responsible for remote cardiac injury and impairment of systolic function observed in vivo.

KEYWORDS

cardiac function, cardiomyocytes, cytoskeleton, doxorubicin, inflammatory cytokines, mitochondria, sex, tumor growth

1 | INTRODUCTION

Cancer has to be considered as a complex syndrome that can result in a series of valuable clinical alterations, including cachexia and progressive loss of body weight, often correlated with a poor prognosis. Cancer growth has also been associated with the occurrence of heart disease (Arámbula-Garza et al., 2016; Ishida et al., 2017; Tilemann, Heckmann, Katus, Lehmann, & Müller, 2018). These alterations have been characterized in detail and have been referred to as "heart cachexia." Among these changes are echocardiographic modifications, a decreased heart size, a loss of the fat surrounding the heart, alterations of cardiomyocytes morphology, and integrity with increased catabolic activity and autophagic triggering. Investigations carried out in human patients with different forms of cancer found an increased incidence of cardiovascular autonomic insufficiency, decreased heart rate variability, an increased resting heart rate, and a decreased resting blood pressure (Guo et al., 2015; Guzzetti, Costantino, Vernocchi, Sada, & Fundarò, 2008; Lainscak, Dagres, Filippatos, Anker, & Kremastinos, 2008; Seviiri et al., 2018). In addition, it is well-known that several agents capable of at least partially impairing tumor growth also exert a plethora of unwanted effects, including heart failure (HF). The most described chemotherapy agent able to induce cardiopathy is the anthracycline doxorubicin (DOXO), a drug of widespread use in the clinical practice since many years and capable to exert antitumor activity against several different forms of cancers thanks to its DNA intercalating activity. Importantly, short or long term "toxic effects" either of cancer per se or of anticancer treatment are still a matter of study because the protection towards paraneoplastic toxic syndrome, including cardiac cachexia, or unwanted side effects of anticancer drugs, such as DOXO, are still an objective of anticancer research, that is finalized to lower tumor growth minimizing toxic insults.

In this study we hypothesized that the deterioration of cardiac functions observed in patients with cancer, regardless of chemotherapy, could be due to the alterations induced by inflammatory cytokines associated with tumor growth on cytoskeleton and mitochondrial network of cardiomyocytes.

2 | MATERIALS AND METHODS

2.1 | Cell culture and treatments

Cardiomyoblast H9c2 derived from female rat were purchased from the American Type Culture Collection (ATCC, Manassas, VA) and maintained at 37°C in Dulbecco's modified Eagle's medium with 10% fetal bovine serum (FBS; Thermo Fisher Scientific, Waltham, MA). H9c2 cells were serum starved and treated with 1 μM retinoic acid (Sigma-Aldrich, Saint Louis, MO) for 48 hr and before and during treatment with 50 ng/ml recombinant rat cytokines tumor necrosis factor α (TNF-α), interferon γ (IFN-γ), interleukin 1β (IL-1β), IL-8, (R&D Systems, Minneapolis, MN) for additional 48 hr.

Low passage-number cell line CT26, isolated for the first time from BALB/c female mice (Corbett, Griswold, Roberts, Peckham, & Schabel, 1975) and obtained from ATCC, was maintained at 37°C, with 5% CO_2 under fully humidified conditions in Roswell Park Memorial Institute-1640 medium (Lonza, Atlanta, GA) supplemented with 10% FBS (EuroClone, Milan, Italy) in the presence of penicillin and streptomycin.

2.2 | Animal welfare and ethics statement

Animal studies are performed in compliance with the Animal Research: Reporting of In Vivo Experiments guidelines (McGrath, Drummond, McLachlan, Kilkenny, & Wainwright, 2010; McGrath & Lilley, 2015) and the European directives (2010/63/EU). Animals were anesthetized with isoflurane before being killed by cervical dislocation. All efforts were made to minimize animal suffering. Mice were housed in groups of three adults per cage and maintained in the standardized conditions in our animal facility at 22 ±2°C room temperature, 40 ± 5% relative humidity and a 12-hr light/dark cycle with dawn/dusk effect, water, and standard pathogen-free chow diet provided ad libitum.

2.3 | Mouse experiments

Female BALB/c mice purchased from Charles River (Calco, Italy) were housed in the animal facility at the Istituto Superiore di Sanità (Rome, Italy) and manipulated in accordance with the local Ethical Committee guidelines. 2×10^6 CT26 cells were injected subcutaneously (s.c.) to induce a subcutaneous tumor. To suppress tumor growth, mice were treated intravenously (i.v.) with DOXO. To avoid both acute and chronic DOXO-mediated cardiotoxicity (Abdullah et al., 2019), a fractionated dose of DOXO (10 mg/kg) was administered once a week for 2 weeks and then cardiac function and structure were evaluated 2 weeks after the initiation of treatment. The body weight of the mice was assessed every day after tumor implantation, and the tumor length and width were measured using a digital caliper once the tumor was palpable. For the analysis of the drug effects, tumors were removed to calculate the body weight as the whole body weight minus the tumor

weight. Three independent experiments considering six mice in each experimental group were performed.

2.4 | RNA preparation and the quantitative real-time polymerase chain reaction

Total RNA was extracted from tumor tissue by using TRIzol (Thermo Fisher Scientific, Waltham, MA) and purified by using RNA purelink mini kit (Invitrogen; Life Technologies, Monza, Italy). The concentration and purity of the RNA solution were determined by using a NanoDrop spectrophotometer (Thermo Fisher Scientific), whereas its overall quality was analyzed using the Agilent 2100 bioanalyser with an RNA LabChip (RNA 6000 Nano kit; Agilent, Santa Clara, CA). Complementary DNA (cDNA) was obtained by random primers and ThermoScript reverse transcriptase (Thermo Fisher Scientific) or by using the high capacity cDNA Archive kit (Applied Biosystems Inc., Foster City, CA). Messenger RNA (mRNA) expression levels for evaluated genes were quantified by using the SensiMix SYBR (Quantace, London, UK) or TaqMan gene expression assays (Applied Biosystems). Quantitative real-time polymerase chain reaction (qRT-PCR) analysis was performed using the 7500 Real-Time PCR system (Applied Biosystems). The ΔC_t was used for statistical analysis, and the treated group values were presented as fold of control mean value.

2.5 | Echocardiography

Mice were anesthetized with Isoflurane (1.5% in 100% of oxygen) and placed in a supine position on a heated operating table to maintain core body temperature at 37°C. Echocardiography (SONO-LINE G50; Siemens AG, Erlangen, German), was performed as described by Patrizio et al. (2007). Briefly, the chest was shaved using a chemical hair remover and warmed ultrasound gel was applied to the surface of the thorax to optimize the visibility of the cardiac chambers. Left ventricular end-diastolic (LVEDD) and end-systolic (LVESD) diameters were measured from a M-mode image of a parasternal short axis view at the level of the papillary muscles. The percentage of change fractional shortening (FS) were measured as follows: FS (%) = ([LVEDD−LVESD]/LVEDD) × 100.

2.6 | Histological analysis

Hearts were fixed in 10%-buffered formalin (Bio Optica, Milan Italy), embedded in paraffin and cut into 5 μm sections. Histological analysis was performed as described previously (Marano et al., 2004). Specifically, LV sections were stained by the Sirius red/picric acid method to determine LV fibrosis by quantitative morphometry (Morphometric; Universal Imaging Corporation, Downingtown, PA).

2.7 | Blood for assay of serum

Blood was collected from the retro-orbital venous sinuses of mice before sacrifice. The sample was allowed to clot for 45 min (to facilitate the removal of all the platelets and precipitates) and then centrifuged at 10,000g for 15 min at +4°C. The serum was stored at −80°C before assay.

2.8 | Total antioxidant capacity

Evaluation of the combined nonenzymatic antioxidant capacity was performed by total antioxidant capacity (TAC) colorimetric assay Kit (BioVision Inc., Milpitas, CA), which measures the sample's capacity to convert Cu^{+2} to Cu^{+1}, following the manufacturer's instructions. The results are expressed in nmol Cu^{2+} reduced.

2.9 | Quantification of cytokines

To quantify cytokine levels, a multiplex assay was used to measure TNF-α, IL-1β, IFN-γ, IL-6, and IL-8 levels in each serum sample by using LXSAMSM-05 kit (R&D Systems). Plates were read on a Magnetic Luminex Screening Assay by Bio-Rad Bio-Plex (Hercules, CA) 100 sn LX 10005039304 instrument. Values of the standard curve are compared with the values provided by the manufacturer of the kits used and not exceed a coefficient of variation of 15%. The results were expressed as pg/ml.

2.10 | Quantification of troponin I and B-type natriuretic peptide)

To quantify troponin I type 3 and B-type natriuretic peptide (BNP) we used enzyme-linked immunosorbent assay kit (Cloud-Clone Corp., Katy, TX) following the manufacturer's instructions. The results were expressed as pg/ml.

2.11 | Western blot analyses

Tissues were lysed in lysis buffer containing 10 mM Tris-HCl (pH 7.4), 5 mM ethylenediaminetetraacetic acid, 5 mM egtazic acid, 1% Triton X-100, 10 mM NaF, 130 mM NaCl, 0.1% sodium dodecyl sulfate (SDS), and 0.1% sodium deoxycholate and allowed to stand for 30 min at 4°C. The lysate was centrifuged for 5 min at 14,000 rpm to remove the debris. After evaluation of the protein concentration by DC Protein Assay Kit (Bio-Rad, Milan, Italy) the lysate was subjected to 10% SDS-polyacrylamide gel electrophoresis. Proteins were electrophoretically transferred into polyvinylidene difluoride membranes (Bio-Rad). Membranes were blocked with 5% defatted dried milk in Tris-buffered saline, containing 0.5% Tween 20 and probed with LC3 or with phospho-ULK1 (Ser 777) rabbit polyclonal anti-human (both Sigma-Aldrich). As a control, the membrane was incubated with specific antibody anti-actin monoclonal antibody (Mab; Santa Cruz Biotechnology, Dallas, TX). Bound antibodies were visualized with horseradish peroxidase-conjugated antirabbit immunoglobulin G (IgG; Sigma-Aldrich) or anti-mouse IgG (Sigma-Aldrich) and immunoreactivity assessed by chemiluminescence reaction, using the enhanced chemiluminescence western detection system (Millipore, Burlington, MA). Densitometric scanning analysis was performed by Mac OS X (Apple Computer International), using the

NIH Image 1.62 software. The density of each band in the same gel was analyzed, values were totaled, and then the percent distribution across the gel was detected.

2.12 | ATP determination

To quantify ATP in control and treated-H9c2 cells we used a bioluminescence assay (Thermo Fisher Scientific) following the manufacturer's instructions. This ATP determination assay is extremely sensitive and it is based on the luciferase's absolute requirement for ATP in producing light (emission maximum ~560 nm at pH 7.8).

2.13 | Immunofluorescence

Cells were fixed with 4% paraformaldehyde and then permeabilized by 0.5% (vol/vol) Triton X-100 as reported (Matarrese et al., 2016). The following primary and secondary antibodies were used: Mouse MAb anti-myosin (Abcam, Cambridge, UK), rabbit polyclonal antibody anti-TOM20 (Santa Cruz Biotechnology), mouse Mab anti-mitochondria (Chemicon - Fisher Scientific, part of Thermo Fisher Scientific), and/or rabbit polyclonal antibody anti-hFIS, AlexaFluor 488-conjugated anti-mouse (Invitrogen, Carlsbad, CA), and AlexaFluor 594-conjugated anti-rabbit IgG (Invitrogen, Temecula, CA). For F-actin detection, cells were stained with tetramethylrhodamine (TRITC)-phalloidin (Sigma-Aldrich, Saint Louis, MO) for 30 min at room temperature. After washing, all the samples were counterstained with Hoechst 33258 (Sigma-Aldrich) and then mounted in glycero/phosphate-buffered saline (PBS; ratio 1:1; pH 7.4). The images were acquired by intensified video microscopy with an Olympus fluorescence microscope (Olympus Corporation of the Americas), equipped with a Zeiss charge-coupled device (CCD) camera (Carl Zeiss, Oberkochen, German).

2.14 | Morphometric analysis

Quantitative evaluations of mitochondrial fragmentation and cell shape alterations were carried out by evaluating at least 50 cells at the same magnification (×1,300). Morphometric analysis was performed by using the ImageJ to measure the average mitochondrial area. To this purpose, red green blue (RGB) images were processed using a custom-written ImageJ macro containing plug-ins that calculate the average area of the mitochondrial particles throughout the cell cytoplasm using the outlines algorithm of the "Analyze Particles" function. The macro-assisted algorithm was set to measure all particle sizes larger than the background pixelation, but smaller than the average nuclear size. The average mitochondrial area is expressed as pixel^2.

2.15 | Flow cytometry

2.15.1 | Mitochondrial membrane potential

The mitochondrial membrane potential of controls and treated H9c2 cardiomiocytes were studied by using 5-5′,6-6′-tetrachloro-1,1′,3, 3′-tetraethyl benzimidazole-carbocyanine iodide probe (JC-1; Molecular Probes, Eugene, OR), as described (Matarrese et al.,

2005). In line with this method, living cells were stained with 10 μM of JC-1. Tetramethylrhodamine ester 1 μM (TMRM; Molecular Probes) was also used to confirm data obtained by JC-1 (not shown).

2.15.2 | Mitochondrial reactive oxygen species

Cells (5×10^4) were incubated with 5 μM MitoSOX (red mitochondrial superoxide indicator, Thermo Fisher Scientific) in complete medium, for 30 min at 37°C.

2.15.3 | Fission proteins

Cells were fixed with 4% paraformaldehyde (Carlo Erba, Milano, Italia) and then permeabilized by 0.5% Triton X-100 (Sigma-Aldrich). After washing, cells were incubated with the following polyclonal antibodies for 1 hr at 4°C: Anti-MNF2 (Cell Signaling; New England Biolabs, Ipswich, MA), anti DRP1 (Cell Signaling), anti-phospho DLP1 (Cell Signaling, Leiden, The Netherlands) and hFIS (Abcam). After washing, cells were incubated with anti-rabbit AlexaFluor 488-conjugated (Thermo Fisher Scientific) for an additional 45 min at 37°C. Cells were then washed in PBS and immediately analyzed on a cytometer. Acquisition of the samples was performed on a FACSCalibur flow cytometer (BD Biosciences, San Jose, CA) equipped with a 488 argon laser and with a 635 red diode laser and at least 30,000 events per sample were run. Data were analyzed using the Cell Quest Pro software (BD Biosciences).

2.16 | Statistical analysis

Results are presented as the mean ± standard deviation (SD). For tests of significance between groups, one-way analysis of variance (ANOVA) was performed. Comparisons between two groups or four groups were performed using the unpaired Student's t test or two-way ANOVA with post hoc tests, respectively (Graphpad software, ver. 5.0). $P < 0.05$ was considered to indicate a statistically significant difference. All measurements were performed at least in three independent experiments.

3 | RESULTS

3.1 | Inflammatory cytokines promote cytoskeleton rearrangement and mitochondrial alterations in cultured cardiomyocytes

In the myocardium, stress-fiber alteration contributes to the development of cardiomyocyte contractile dysfunction and cardiomyopathy (Bravo-Cordero, Magalhaes, Eddy, Hodgson, & Condeelis, 2013).

On this basis, we tested the effects of the main inflammatory cytokines, IFN-γ, TNF-α, IL-6, IL-8, and IL-1β on cultured H9c2 cardiomyocytes. First, we performed a qualitative analysis of the microfilament system organization, responsible for cell contraction, by fluorescence microscopy after cell staining with TRITC-Phalloidin, which recognizes F-actin, and a specific antibody to myosin. As shown in Figure 1, 48 hr of treatment with each of these inflammatory cytokines induced a deep alteration either in actin/myosin

(a)
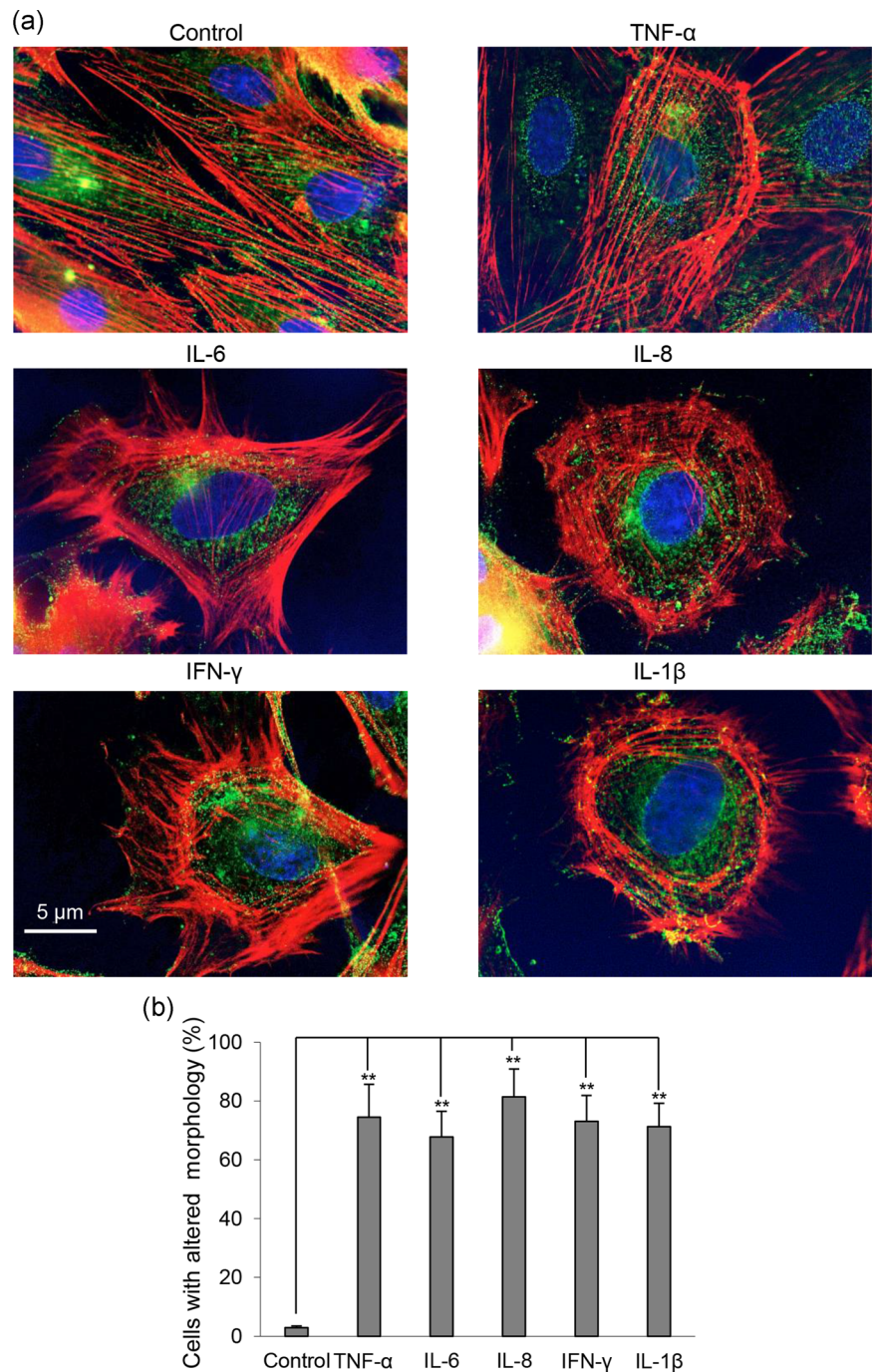
FIGURE 1 Inflammatory cytokines promote cytoskeleton rearrangement in in vitro-cultured cardiomyocytes. (a) Representative micrographs obtained by IVM after TRITC-phalloidin (red)/myosin (green)/Hoechst (blue) triple staining of H2c9 cardiomyocytes untreated (control) or treated for 48 hr with 50 ng/ml IFN-γ, TNF-α, IL-6, IL-8 or IL-1β. (b) Bar graph shows morphometric analysis results. In ordinate the percentage of the cells with an altered shape in comparison to control cells. **$p < 0.01$. IFN-γ: interferon γ; IL-6: interleukin 6; IVM: in vitro maturation; TNF-α: tumor necrosis factor α; TRITC: tetramethylrhodamine

organization or in cell shape. In particular, cardiomyocytes challenged with the above cytokines lost their bipolar shape along with the compromised orientation of the stress fibers, as also demonstrated by the morphometric analysis (bar graph in Figure 1b).

3.2 | Inflammatory cytokines induce mitochondrial network alterations and upregulation of phospo-DRP1 and hFIS in in vitro-cultured cardiomyocytes

An increasing number of studies place mitochondrial dysfunction as a key event in diseases affecting the heart. In particular, mitochondria form a highly interconnected and dynamic network in cardiomyocytes and provide necessary ATPs for the smooth functioning of the heart (Kuzmicic et al., 2011). Thus, we investigated the mitochondrial network in H9c2 cardiomyocytes undergoing treatment with IFN-γ, TNF-α, IL-6, IL-1β, and IL-8. We found that although each of these cytokines induced mitochondrial fragmentation (Figure 2a), normally associated with dysfunctional mitochondria (Disatnik et al., 2013), as confirmed by the morphometric analysis performed by the ImageJ software to measure average mitochondrial area in cells stained with an anti-TOM20 Ab (Figure 2b).

In mammals, at least two proteins, the dynamin-related protein 1 (DRP1) and the mitochondrial outer membrane protein hFIS1,
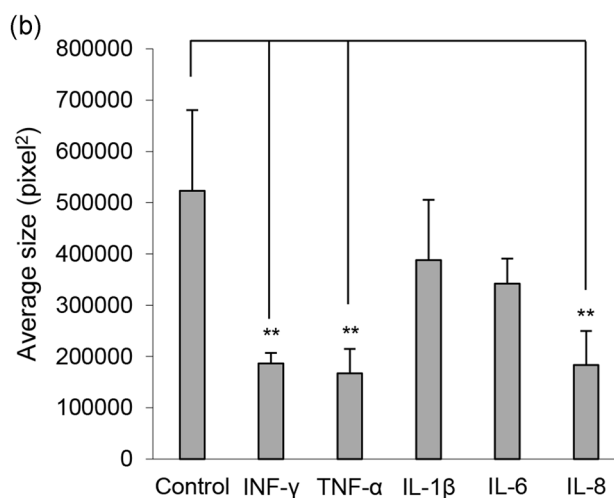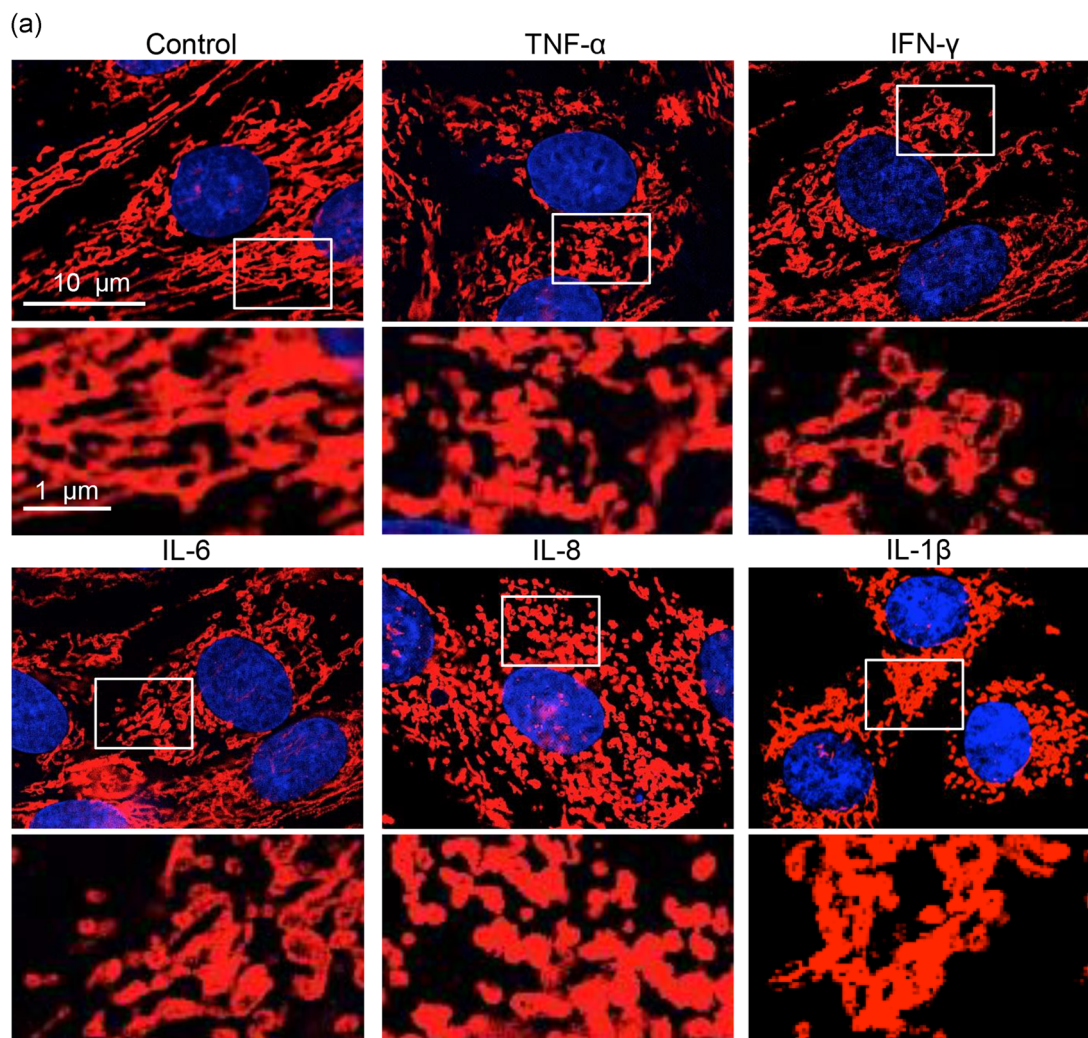
FIGURE 2 Inflammatory cytokines induce mitochondrial network alterations in in vitro-cultured cardiomyocytes. (a) Representative micrographs obtained by IVM showing the mitochondrial network of H2c9 cardiomyocytes untreated (control) or treated for 48 hr with 50 ng/ml IFN-γ, TNF-α, IL-6, IL-8, or IL-1β after staining with anti-TOM20 (red) and counterstaining with Hoechst (blue). In the bottom pictures, magnification of the boxed areas. (b) Bar graph showing morphometric analysis performed by using the ImageJ software. In ordinate average mitochondrial area is expressed as pixel^2. Data are reported as mean value ± *SD* of the results obtained by analyzing at least 30 cells for each sample. IFN-γ: interferon γ; IL-6: interleukin 6; IVM: in vitro maturation; *SD*: standard deviation; TNF-α: tumor necrosis factor α

participate in mitochondrial fission. Thus, we analyzed by flow cytometry phosphorylated active form of DRP1 (p-DRP1), and hFIS1, which are recruited to the mitochondrial outer membrane during mitochondrial fission (Yoon, Krueger, Oswald, & McNiven, 2003). As shown in Figure 3, treatment of each inflammatory cytokine-induced, although to a different extent, an increase of both p-DRP1 (Figure 3a) and hFIS1 (Figure 3b). According to this, immunofluorescence analysis performed in cells doubly stained with an anti-TOM20 antibody and anti-hFIS antibody has shown that hFIS1 was localized at mitochondria level especially in cells treated with IL-8, IFN-γ, or TNF-α (see yellow fluorescence). The relocalization of hFIS1 at mitochondria was significantly less evident in cells treated with IL-6 and IL-1β.

3.3 | Inflammatory cytokines induce an increase of the mitochondrial membrane potential and mitochondrial reactive oxygen species production in in vitro-cultured cardiomyocytes

Accumulating amounts of evidence indicate that the mitochondrial fragmentation and fission represent important contributing factors to reactive oxygen species (ROS) overproduction and alterations of mitochondrial membrane and ATP production (Shenouda et al., 2011; Yu, Jhun, & Yoon, 2011). According to this, we found that cytokine-induced mitochondrial network fragmentation was paralleled by hyperpolarization of mitochondrial membrane (Figure 4a,b) and a significant increase of mitochondrial ROS production (Figure 4c,d). As expected, treatment of cardiomyocytes with inflammatory cytokines also induced a significant decrease (~40%) of ATP content (control, 2.63 ± 0.44; TNF-α, 1.47 ± 0.21; IL-6, 1.59 ± 0.34; IL-8, 1.54 ± 0.31; IFN-γ, 1.61 ± 0.28; IL-1β, 1.67 ± 0.41 nmol × 10^6 cells).

## 3.4 | colorectal cancer tumor growth induces very early heart dysfunction

Subsequently, we wanted to test our hypothesis in an in vivo model. To investigate the effects of tumor growth on cardiac function we transplanted sc CT26 colorectal cancer (CRC) cells into female BALB/c mice. In parallel, experiments with DOXO, a well-known potent chemotherapeutic agent (Baxter-Holland & Dass, 2018; Tran, DeGiovanni, Piel, & Rai, 2017), were also carried out to suppress tumor growth. CT26-bearing mice were subjected to a short treatment with a fractionated dose of DOXO, that is 10 mg/kg given iv once a week for 2 weeks (Figure S1). In untreated animals, tumors grew progressively up to 25 days along with no significant changes in body weight or food intake either during or at the end of the experiment (Figure 5a,c). Similarly, no signs of cachexia were detected (data not shown). As expected, DOXO was able to inhibit significantly cancer growth (Figure 5a). In addition, moderate weight loss and slightly increased food intake, indicative of hyperphagia occurrence, were observed in DOXO-treated tumor-bearing mice with respect to the untreated tumor-bearing mice or healthy mice subjected to DOXO treatment (Figure 5b,c).

To assess the influence of tumor growth and/or DOXO treatment on LV remodeling and function, mice were killed after 25 days tumor cells transplantation and a series of analyses were performed. As shown in Figure 6a, echocardiographic evaluations carried out immediately before the sacrifice of the animals and revealed that CT26-bearing mice had a reduced FS when compared with the healthy control ($20.1 \pm 2.3\%$ and $34.3 \pm 2.1\%$, respectively). Upon DOXO treatment for 2 weeks, we found that this drug, along with the inhibition of tumor growth, was able to counteract early tumor-associated decrease of FS ($28.2 \pm 1.1\%$ in DOXO-treated CT26-bearing mice vs. $20.1 \pm 2.3\%$ in untreated CT26-bearing mice; Figure 6a). In contrast, no evidence of cardiac remodeling was found in CT26-bearing mice treated with DOXO. In fact, LV diastolic wall thickness remained unchanged (Figure 6b) as well as mRNA levels of β-MHC genes (Figure 6c). By contrast, the levels of natriuretic peptide A (NPPA) mRNA found decreased in untreated CT26-bearing mice versus healthy mice, were restored in CT26-bearing mice undergoing DOXO treatment (Figure 6d). Importantly, in our experimental conditions, the short-term administration of DOXO in healthy mice caused no cardiac dysfunction, remodeling or fibrosis, due to the myocardial interstitial collagen reorganization, as revealed by echocardiographic, biochemical and histological analyses (Figure 6a,b; Figure S2). Of interest, the transcript analysis of the proinflammatory cytokine TNF-α, which disclosed a clear-cut increased production in ventricles of tumor-bearing mice, also revealed a significant decrease in DOXO-treated CT26-bearing mice (Figure 6e). Moreover, the levels of IFN-γ and IL-8 remained unchanged whereas the levels of IL-6 and IL-1β increased in tumor-bearing animals (Figure S3). As BNP and troponin I are systemic biomarkers for the prediction of cardiac injury, we further evaluated these parameters in plasma. We found the higher levels of BNP in CT26-bearing mice with respect to the healthy counterpart and observed a significant decrease in CT26-bearing mice treated with DOXO (Figure 6f). In contrast, the small difference found in plasma level of troponin I among the animal groups was not significant (Figure 6g). These results highlight the role of tumor development in dictating cardiac damage and the absence of significant adverse cardiac effects of the short-term treatment with DOXO.

3.5 | Tumor-induced heart damage correlates with systemic inflammation

Chronic systemic inflammation is proposed as an underlying mechanism for the development of cardiac injury (Bye et al., 2016). Thus, in light of the in vitro data, we investigated the expression of the major systemic and tumor-associated inflammatory cytokines, such as TNF-α, IL-1β, IL-6, IL-8, and IFN-γ, reported to be implicated in the development of cardiac dysfunction (Mann, 2002; Zhao et al., 2013). Analysis of tumor samples from CT26-bearing mice, in the absence and presence of DOXO treatment, revealed significant expression of IL-1β and detectable IFN-γ transcripts in untreated animals. DOXO treatment resulted in a significant increase in transcripts of both cytokines (Figure 7a). Conversely, while the
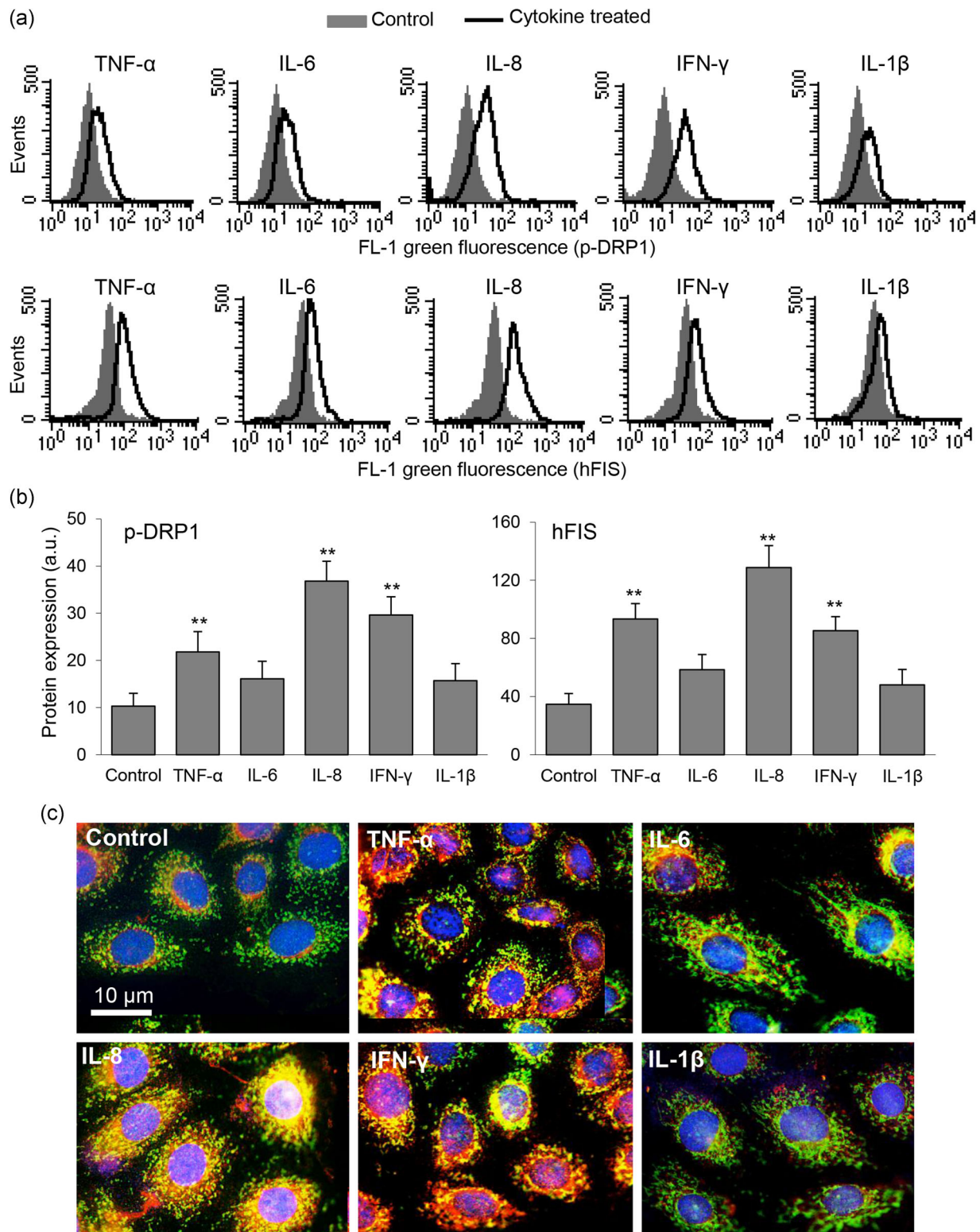
FIGURE 3 Inflammatory cytokines induce upregulation of phospo-DRP1 and hFIS in in vitro-cultured cardiomyocytes. (a) Representative histograms of the cytofluorimetric analysis of expression level of p-DRP1 (first row) and hFIS (second row). (b) Bar graphs showings the mean ± SD of the results obtained from three independent experiments expressed as median fluorescence intensity. **$p < 0.01$. (c) Representative micrographs obtained by IVM showing mitochondrial network and hFIS of H2c9 cardiomyocytes untreated (control) or treated for 48 hr with 50 ng/ml IFN-γ, TNF-α, IL-6, IL-8, or IL-1β after staining with anti-mitochondria (green), anti-hFIS (red), and counterstaining with Hoechst (blue). Note yellow fluorescence in cells treated with cytokines that indicate mitochondrial localization of hFIS. DRP1: dynamin-related protein 1; IFN-γ: interferon γ; IL-6: interleukin 6; IVM: in vitro maturation; SD: standard deviation; TNF-α: tumor necrosis factor α

(a)

(b)

(c)

(d)
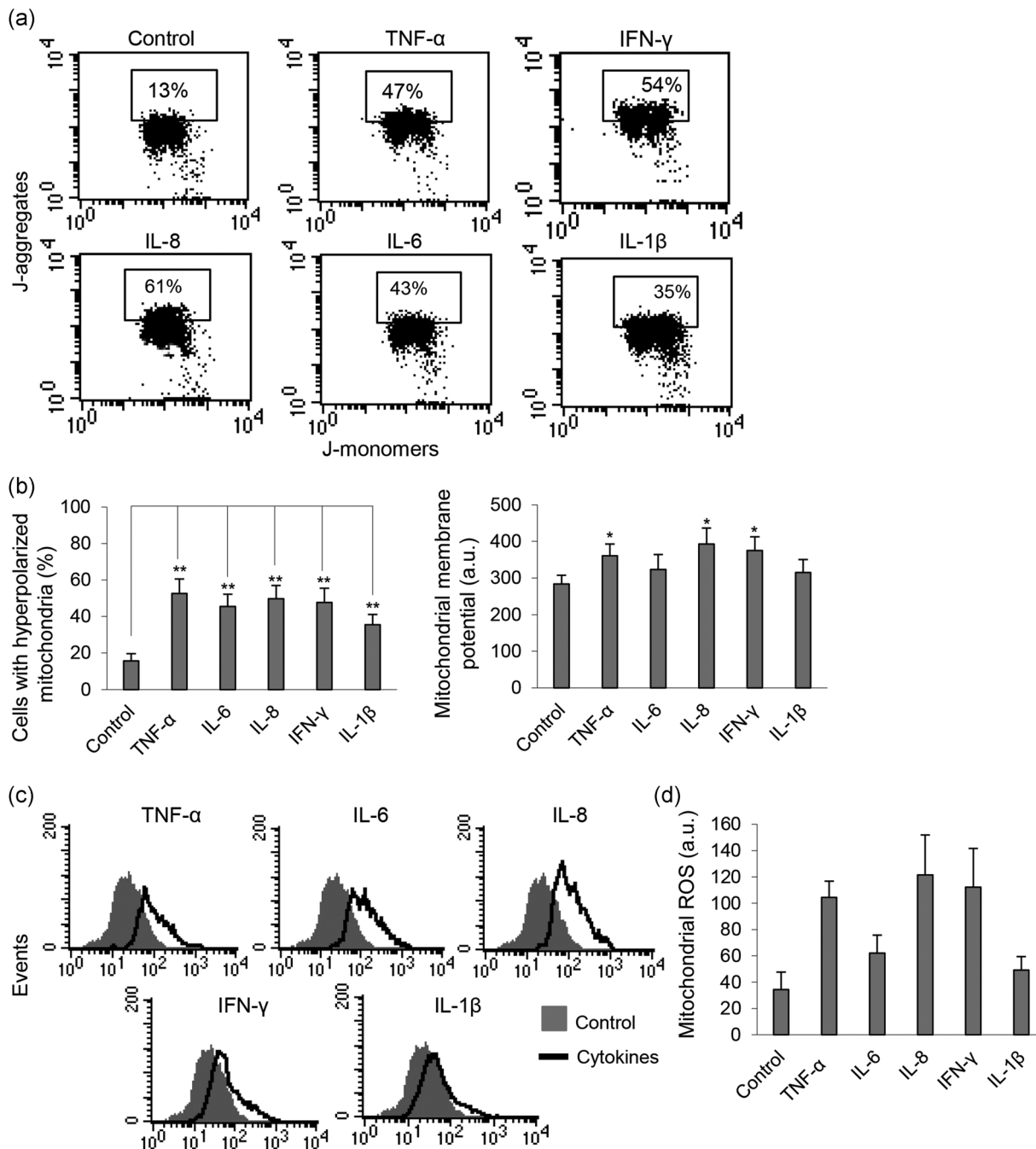
FIGURE 4 Inflammatory cytokines induce an increase of the mitochondrial membrane potential and mitochondrial ROS production in in vitro-cultured cardiomyocytes. (a) Representative dot plots of the cytofluorimetric analysis of MMP, performed by using JC-1. Numbers in the boxed areas indicate the percentage of cells with high MMP. (b) Left panel. Bar graph showing the results of the analysis of MMP obtained by using JC-1 from three independent experiments and reported as the percentage ± SD of cells with hyperpolarized mitochondria. Right panel. Bar graphs showings the mean ± SD of the results obtained by using TMRM from three independent experiments expressed as median fluorescence intensity. (c) Representative histograms of the cytofluorimetric analysis of mitochondrial ROS, performed by using the MitoSox probe. (d) Bar graph shows the mean ± SD of the results obtained from three independent experiments expressed as median fluorescence intensity. **$p < 0.01$. IFN-γ: interferon γ; IL-6: interleukin 6; MMP: mitochondrial membrane potential; ROS: reactive oxygen species; SD: standard deviation; TMRM: tetramethylrhodamine; TNF-α: tumor necrosis factor α

expression of IL-1β and IFN-γ levels was important in spleens of untreated tumor-bearing animals, upon DOXO treatment IFN-γ levels were strikingly downmodulated and IL-1β was found unchanged. Similarly to that observed in tumors, IL-6, as well as IL-8,

remained undetectable (Figure 7b). Next, the levels of the cytokines were assayed in the plasma of all animals included in this study. As shown in Figure 7c, while a modest, but significant, increase of IFN-γ, TNF-α, and IL-6 were found in the plasma of tumor-bearing mice in
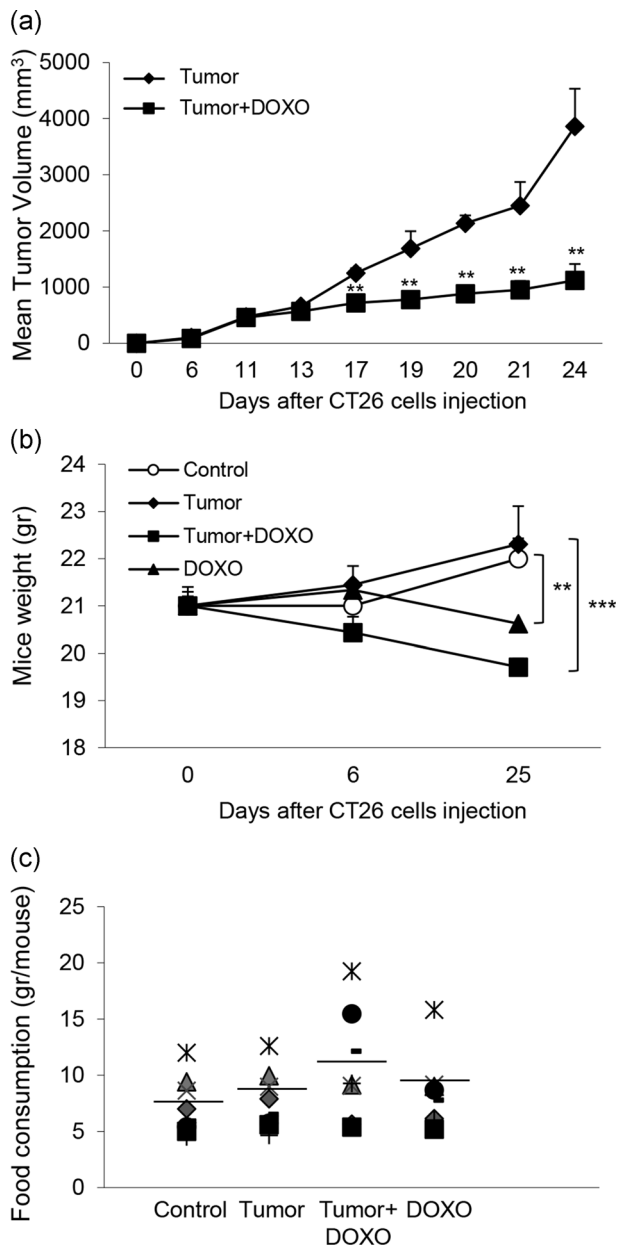
FIGURE 5 Effect of DOXO on tumor burden in the CT26 tumor-bearing mice. (a) BALB/c mice have injected sc with 2×10^6 CT26 cells and tumor size was measured over time. After 6 and 13 days, mice have treated iv with DOXO (10 mg/kg). Data represent the mean tumor volume ± *SD*. One representative experiment out of three is shown. **p ≤ 0.01 versus untreated mice bearing the CT26 tumor. (b) The body weight of mice was expressed as total weight minus tumor weight and measured before tumor cells inoculation (Day 0), before DOXO treatment when tumors were palpable (Day 6) and at the end of the study (Day 25). (c) Effect of DOXO on cumulative food intake in mice. Food consumption was monitored every 3 days and the mean of total measures is shown. DOXO: doxorubicin; s.c.: subcutaneously; *SD*: standard deviation; i.v.: intravenously

comparison to the healthy counterpart, these animals exhibited a highly significant up-modulation of plasmatic IL-8. Of interest, treatment with DOXO of mice with tumor significantly reduced the plasmatic level of the above cytokines, in particular, IL-8. By contrast,

no significant differences in the plasma levels of IL-1β were found among the diverse experimental groups (Figure 7c). These data suggest, on one hand, the occurrence of systemic inflammation in the presence of tumor and, on the other hand, the capability of DOXO to reduce a systemic production of inflammatory cytokines, specifically IFN-γ in spleen and IL-8 in plasma.

To correlate the increase of systemic proinflammatory cytokines in CT26-bearing mice with the systemic oxidative stress, we further evaluated the TAC, which is indicative of the abundance of antioxidant molecules and enzymes in the blood are able to counteract the effects of ROS/reactive nitrogen species (Du, Anderson, Lortie, Parsons, & Bodnar, 2013). As shown in Figure 7d, a reduction of TAC was observed in tumor-bearing animals, which was partially counteracted by treatment with DOXO.

3.6 | Involvement of autophagy in tumor-induced heart damage

Cardiac homeostasis is also regulated by autophagy. Therefore, we evaluated the occurrence of autophagy in both ventricle tissue and explanted tumors from CT26-bearing mice either untreated or treated with DOXO. Western blot analysis of LC3 in ventricle tissue revealed an increase of LC3-II, the lipidated form of LC3, in tumor-bearing mice undergoing DOXO treatment in comparison with the untreated counterpart, clearly suggesting the capability of DOXO to increase autophagy (Figure 8a). Surprisingly, we also found a significant increase in phospho-ULK1 (p-ULK, Ser 777). Ser 777, a phosphorylation site, is known to be a 5′ adenosine monophosphate-activated protein kinase (AMPK) phosphorylation sites in ULK1 (Figure 8a; Kim, Kundu, Viollet, & Guan, 2011). In contrast, we did not observe any significant difference of autophagic levels in explanted tumors from untreated or treated tumor-bearing mice (Figure 8b). This finding suggests that the autophagy is critical at heart but not at tumor level for DOXO activity.

4 | DISCUSSION

Cardiac dysfunction represents a serious complication in patients with cancer. Although cardiotoxicity is generally related to chemotherapy and other anticancer therapies, the impact, molecular mechanisms and biological basis of the effects induced by tumor growth on cardiac functions, regardless of therapy, still remain unclear and little investigated.

The close link we hypothesized between early heart dysfunction and inflammatory signals was verified in an in vitro experimental model. Treatment with IL-1β, IFN-γ, TNF-α, IL-6, or IL-8, induced in cardiomyocytes severe alterations of actomyosin cytoskeleton distribution, of mitochondrial network organization, and of mitochondrial membrane potential. In particular, we observed an increase of mitochondrial membrane potential in agreement with the fact that the above inflammatory cytokines (at least at the concentrations and
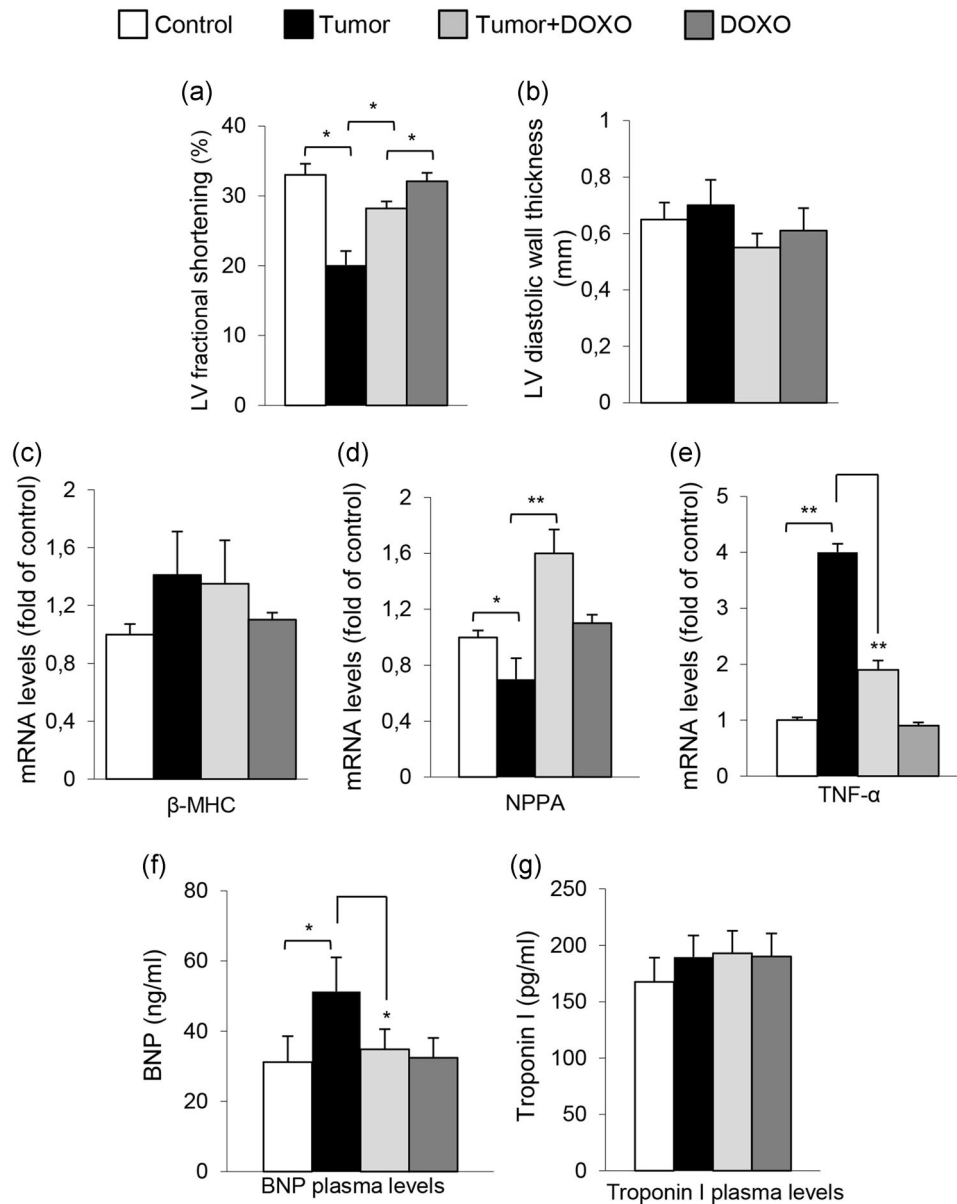
FIGURE 6 CRC tumor growth induces very early cardiac dysfunction. (a) CT26-bearing mice display a reduced FS when compared with the untreated control. DOXO administration prevented the development of cardiac dysfunction. Also, doxorubicin alone did not affect cardiac function. (b) Neither cancer growth nor DOXO altered LV diastolic wall thickness, an echocardiographic marker of cardiac remodeling. (c) mRNA levels of β-MHC (d) NPPA, and (e) TNF-α were assessed from heart tissue samples by q-PCR after being normalized by the mRNA level of GAPDH. Untreated heart tissue samples from BALB/c mice (control) were used as negative control. Quantitative evaluation of (f) BNP and (g) troponin I in animal plasma was performed by ELISA assay and expressed as pg/ml. Data reported are the mean ± *SD* of the results obtained by analyzing at least six animals in three independent experiments; each experimental analysis was performed in triplicate. *$p < 0.05$, **$p < 0.01$. BNP: B-type natriuretic peptide; CRC: colorectal cancer; DOXO: doxorubicin; ELISA: enzyme-linked immunosorbent assay; FS: fractional shortening; LV: left ventricular; mRNA: messenger RNA; NPPA: natriuretic peptide A ; q-PCR: quantitative polymerase chain reaction; *SD*: standard deviation; TNF-α: tumor necrosis factor α

treatment times we used) did not induce cell death. By contrast, Hahn et al. (2014) reported a loss of mitochondrial membrane potential in 3T3 cells treated with inflammatory cytokines. This discrepancy could be due to the different cell type considered.

Noteworthy, cardiomyocytes also exhibited a fragmentation of mitochondrial network, that is mitochondria fission, when treated with the above cytokines, particularly evident in IL-8-treated cells. It

was hypothesized that these alterations may impact on heart and vasculature function, with the potential to represent biological determinants in the health of the heart in patients with tumor (Ong, Kalkhoran, Cabrera-Fuentes, & Hausenloy, 2015). Altered mitochondrial biogenesis and fragmentation were also observed in human and animal model of HF, and seem to be caused by changes in expression of proteins that regulate mitochondrial dynamics, such as
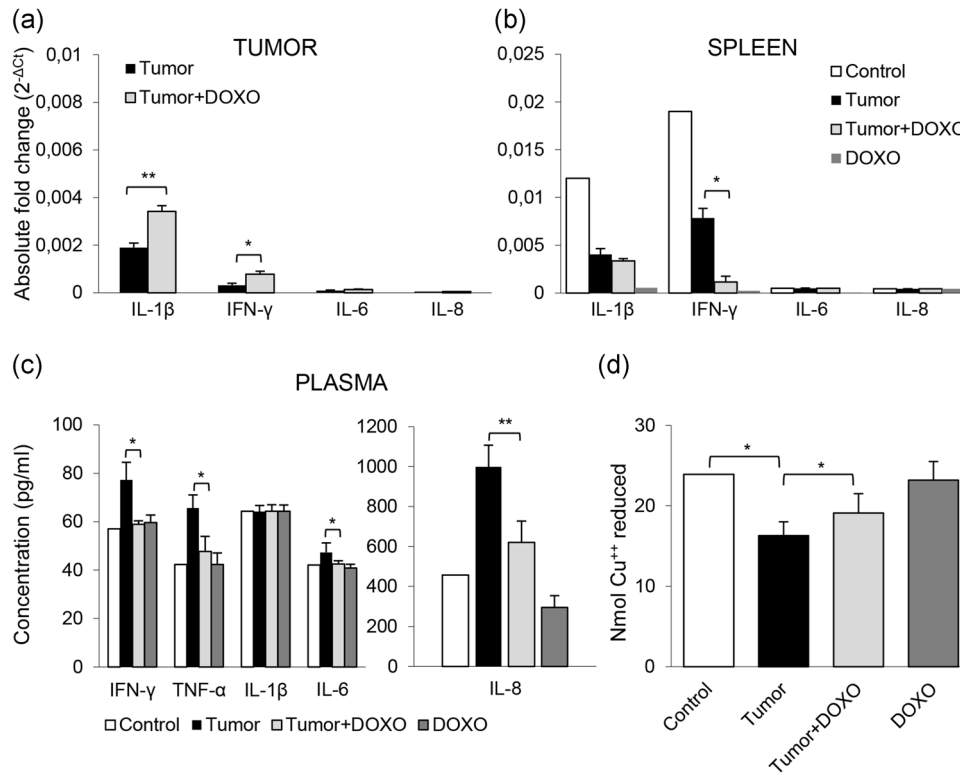
FIGURE 7 Tumor-induced heart damage correlates with systemic immune activation. Effects of DOXO on tissue and systemic cytokines. RNA was purified from tumors (a) and spleen (b) and qRT-PCR for the indicated cytokines was carried out. Histograms represent the absolute mRNA amount normalized to β-actin in samples run in triplicate (mean ± *SD*). One representative experiment of three is shown. (c) Quantitative ELISA of IFN-γ, TNF-α, IL-1β, IL-6, and IL-8 in plasma of healthy mice untreated or treated with DOXO and in mice CT26-bearing tumor, untreated or treated with DOXO. Data are the mean ± *SD* among six animals for each experimental point performed in triplicate. (d) TAC was assayed by using a specific colorimetric test, which measures the total antioxidant power in terms of the sample's ability to reduce copper. Each value reported represents the mean ± *SD* of results obtained by analyzing at least six animals for each experimental point performed in triplicate. *$p < 0.05$, **$p < 0.01$. DOXO: doxorubicin; ELISA: enzyme-linked immunosorbent assay; IFN-γ: interferon γ; IL-6: interleukin 6; mRNA: messenger RNA; qRT-PCR: quantitative real-time polymerase chain reaction; *SD*: standard deviation; TAC: total antioxidant capacity
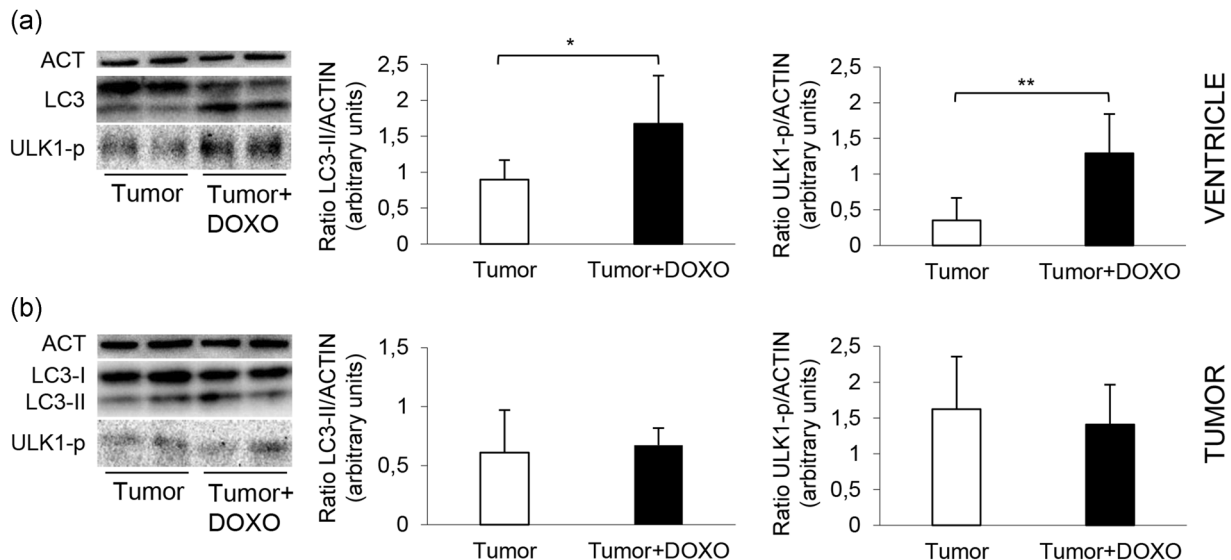
FIGURE 8 Involvement of autophagy in tumor-induced heart damage. Western blot analysis using anti-LC3 and p-ULK (Ser 777) antibodies (a) in ventricle tissue or (b) in explanted tumors from CT26-bearing mice either untreated (tumor) or treated with DOXO (tumor + DOXO). Loading control was evaluated using anti-actin MAb. Two animals representative among six are shown. Bar graphs show densitometric analysis. *$p < 0.05$, **$p < 0.01$. DOXO: doxorubicin; MAb: monoclonal antibody

hFIS, Mitofusin 2, and OPA1. As these factors are known as regulators of mitochondrial metabolism, these changes might be directly related to the decreased capacity to oxidize fatty acid substrates often seen in HF (Brown et al., 2017). The balance between fission and fusion is very important for mitochondrial participation in crucial cellular processes, and disruption of mitochondrial dynamics is emerging as a pathogenetic determinant in prevalent diseases (Dorn, 2015). However, whether the alterations of mitochondrial fusion and fission processes directly cause LV systolic dysfunction or merely constitute a consequence of this remains to be determined (Ventura-Clapier, Garnier, Veksler, & Joubert, 2011).

Our results provided evidence that tumor growth per se reduces cardiac systolic function, which is apparently associated with the systemic inflammation. Our study includes the analysis of control mice and tumor-bearing mice, both treated or not with a paradigmatic anticancer drug, that is DOXO that has been reported to produce both acute and chronic cardiotoxicity (Minotti, Menna, Salvatorelli, Cairo, & Gianni, 2004; Octavia et al., 2012). Strikingly, in our model, the healthy immunocompetent BALB/c mice, administration of DOXO caused no cardiac dysfunction, remodeling or fibrosis, at least in the short term, as revealed by echocardiographic, biochemical, and histological analyses. This discrepancy could be due to: (a) The short-term treatment (once a week for 2 weeks) carried out in the present study, (b) DOXO could induce cardiac alterations after many years from the end of treatment, as sometimes observed in patients with cancer; and (c) the use of female mice in our study. In fact, some papers recently reported a significant sexual dimorphism in the sensitivity to DOXO toxicity (Hequet et al., 2004; Moulin, Piquereau et al., 2015; Štěrba et al., 2013). A critical role of mitochondrial dysfunction, altered energy metabolism, together with altered cardiolipin homeostasis, was hypothesized to play a role in the observed sex differences in vivo (Moulin, Solgadi et al., 2015; Mejia, Cole, & Hatch, 2014). The fact that cancer growth per se was able to interfere with heart activity was also clearly demonstrated by echocardiographic signs of heart function impairment, such as a significant reduction of FS. On this basis, we hypothesized that humoral factors secreted from and/or induced by the tumor could be responsible for promoting LV systolic dysfunction.

Our murine model, characterized by host immunocompetence, allowed us to identify immunological factors, inflammatory responses, and metabolic signals that cannot be investigated in animal models that lack the immunological components, such as nude and severe combined immunodeficient mice. In fact, for preventing rejection of xenografted human cells, immunocompromised mice are usually used. At variance, immune responses and their alterations are nowadays thought to play a key role in tumor development and progression (Budhu, Wolchok, & Merghoub, 2014) so that the immunocompetent tumor-bearing mice have been proposed to represent a suitable model. Accordingly, in our study, host immune response (resulting in an increase of proinflammatory cytokines synthesis at tumor and spleen level) appeared to be observable in tumor-bearing mice. Importantly, this picture of systemic inflammation was tightly correlated to CT26-bearing mice heart dysfunction.

In fact, these animals were characterized by a progressive tumor growth associated to both tissue inflammation (with elevated levels mainly of IL-1β and IFN-γ), and systemic inflammation (with increased inflammatory cytokines such as IL-8, IFN-γ, TNF-α, and IL-6 at the plasma level), and by cardiac systolic dysfunction with a local increase of TNF-α levels.

Cardiac homeostasis is also regulated by autophagy and cardiac-specific reduction of autophagy could result in contractile dysfunction, increased levels of polyubiquitinated proteins and increased apoptosis (Nakai et al., 2007). Moreover, it is possible that autophagy, to prevent protein aggregation, could degrade myofibrillar proteins cleaved from the sarcomere during cardiac atrophy thus preserving cardiac function. Accordingly, deregulated autophagic processes have been associated with heart dysfunctions, including cardiomyopathies, cardiac hypertrophy, ischemic heart disease, HF, and ischemia-reperfusion injury (Choi, Ryter, & Levine, 2013; Kirshenbaum, 2012). Indeed, in the heart, autophagy activation can be beneficial or detrimental depending on the physiopathological context (Lavandero et al., 2013; Sciarretta, Maejima, Zablocki, & Sadoshima, 2018). Hence, more in general, a differential role for autophagy in acute versus chronic heart disease has been suggested: Short-term activation of autophagy may confer cardiac benefits, whereas sustained autophagy could have detrimental effects (Delbridge, Mellor, Taylor, & Gottlieb, 2017). In our study, ventricle tissues from tumor-bearing mice were found to exhibit a significant decrease of autophagy that was prevented by short-term treatment with DOXO. In this regard, many studies showed that DOXO can upregulate cardiac autophagy contributing to DOXO-dependent cardiotoxicity (Chen et al., 2011; Kobayashi, Xu, Chen, & Liang, 2012; D. L. Li et al., 2016). By contrast, other studies reported that autophagy activation could protect from DOXO-induced cardiotoxicity (Bartlett, Trivedi, & Pulinilkunnil, 2017; S. Li et al., 2014; Pizarro et al., 2016). Anyway, the role of autophagy in DOXO cardiotoxicity is still a matter of debate as it is unclear whether DOXO induces or disrupts the cardiac autophagic activity and if cardiomyocyte autophagy modulation could be beneficial or detrimental. To complicate this scenario, it has also been hypothesized that an increased AMP/ATP ratio could activate AMPK, a sensor a cell energy levels, by phosphorylation at Thr172 (Kim, Kundu, Viollet, & Guan, 2011) and that the active AMPK can stimulate the autophagy activating kinase ULK1 by its direct phosphorylation. This could suggest that, in response to cardiac damage observed in tumor-bearing mice, possibly induced by an inflammatory condition due to the tumor growth, AMPK may enhance autophagy through the direct activation of ULK1 by phosphorylating Ser 777 via a mammalian target of rapamycin independent pathway (Koleini & Kardami, 2017).

All in all, the present study seems to suggest that cancer growth could exert per se, independently from chemotherapy effects, cardiotoxicity at least partially due to a tumor-dependent systemic inflammation that, although could be beneficial for tumor growth control, can also be detrimental for heart integrity and function.

Even if strong evidence suggests that cytokines and other inflammatory molecules, as well as a deregulation of the autophagic

processes, could be involved in the development of cardiac impairment and injury, their causative role in the cardiac dysfunction due to the tumor growth should be further investigated in more detail in animal models and, where feasible, extended in humans.

CONFLICT OF INTERESTS

The authors declare that there are no conflict of interests.

AUTHOR CONTRIBUTIONS

M. B. and S. M. were in charge of in vivo experiments and participated in the analysis of data. B. A. was responsible for cell culture experiments. L. G. was responsible for flow cytometry experiments. M. M. was responsible for autophagy experiments. M. S., D. M., and T. S. were in charge of in vivo experiments and participated in the analysis of data. M. P. was responsible for RNA preparation and quantitative real-time polymerase chain reaction. W. M. participated in the design of the study and the interpretation of data. G. M. was responsible for echocardiography, conceived the idea, participated in the design of the study, and participated in the analysis and interpretation of data. P. M., L. G., and G. M. conceived the idea, participated in the design of the study, participated in the analysis and interpretation of data, and drafted the manuscript. All authors read and approved the final manuscript.

ORCID

Paola Matarrese 🆔 http://orcid.org/0000-0001-5477-3752

REFERENCES

Abdullah, C. S., Alam, S., Aishwarya, R., Miriyala, S., Bhuiyan, M. A. N., Panchatcharam, M., ... Bhuiyan, M. S. (2019). Doxorubicin-induced cardiomyopathy associated with inhibition of autophagic degradation process and defects in mitochondrial respiration. *Scientific Report, 9,* 2002. https://doi.org/10.1038/s41598-018-37862-3

Arámbula-Garza, E., Castillo-Martínez, L., González-Islas, D., Orea-Tejeda, A., Santellano-Juárez, B., Keirns-Davies, C., ... Pablo-Santiago, R. (2016). Association of cardiac cachexia and atrial fibrillation in heart failure patients. *International Journal of Cardiology, 223,* 863–866. https://doi.org/10.1016/j.ijcard.2016.08.318

Bartlett, J. J., Trivedi, P. C., & Pulinilkunnil, T. (2017). Autophagic dysregulation in doxorubicin cardiomyopathy. *Journal of Molecular and Cellular Cardiology, 104,* 1–8. https://doi.org/10.1016/j.yjmcc.2017.01.007

Baxter-Holland, M., & Dass, C. R. (2018). Doxorubicin, mesenchymal stem cell toxicity and antitumour activity: Implications for clinical use. *Journal of Pharmacy and Pharmacology, 70*(3), 320–327. https://doi.org/10.1111/jphp.12869

Bravo-Cordero, J. J., Magalhaes, M. A. O., Eddy, R. J., Hodgson, L., & Condeelis, J. (2013). Functions of cofilin in cell locomotion and invasion. *Nature Reviews Molecular Cell Biology, 14*(7), 405–415. https://doi.org/10.1038/nrm3609

Brown, D. A., Perry, J. B., Allen, M. E., Sabbah, H. N., Stauffer, B. L., Shaikh, S. R., ... Gheorghiade, M. (2017). Mitochondrial function as a therapeutic target in heart failure. *Nature Reviews Cardiology, 14*(4), 238–250. https://doi.org/10.1038/nrcardio.2016.203

Budhu, S., Wolchok, J., & Merghoub, T. (2014). The importance of animal models in tumor immunity and immunotherapy. *Current Opinion in Genetics & Development, 24,* 46–51. https://doi.org/10.1016/j.gde.2013.11.008

Bye, A., Wesseltoft-Rao, N., Iversen, P. O., Skjegstad, G., Holven, K. B., Ulven, S., & Hjermstad, M. J. (2016). Alterations in inflammatory biomarkers and energy intake in cancer cachexia: A prospective study in patients with inoperable pancreatic cancer. *Medical Oncology, 33*(6), 54. https://doi.org/10.1007/s12032-016-0768-2

Chen, K., Xu, X., Kobayashi, S., Timm, D., Jepperson, T., & Liang, Q. (2011). Caloric restriction mimetic 2-deoxyglucose antagonizes doxorubicin-induced cardiomyocyte death by multiple mechanisms. *Journal of Biological Chemistry, 286*(25), 21993–22006. https://doi.org/10.1074/jbc.M111.225805

Choi, A. M. K., Ryter, S. W., & Levine, B. (2013). Autophagy in human health and disease. *New England Journal of Medicine, 368*(7), 651–662. https://doi.org/10.1056/NEJMra1205406

Corbett, T. H., Griswold, D. P., Roberts, B. J., Peckham, J. C., & Schabel, F. M. (1975). Tumor induction relationships in development of transplantable cancers of the colon in mice for chemotherapy assays, with a note on carcinogen structure. *Cancer Research, 35*(9), 2434–2439. Retrieved from http://www.ncbi.nlm.nih.gov/pubmed/1149045

Delbridge, L. M. D., Mellor, K. M., Taylor, D. J., & Gottlieb, R. A. (2017). Myocardial stress and autophagy: Mechanisms and potential therapies. *Nature Reviews Cardiology, 14*(7), 412–425. https://doi.org/10.1038/nrcardio.2017.35

Disatnik, M., Ferreira, J. C. B., Campos, J. C., Gomes, K. S., Dourado, P. M. M., Qi, X., & Mochly-Rosen, D. (2013). Acute inhibition of excessive mitochondrial fission after myocardial infarction prevents long-term cardiac dysfunction. *Journal of the American Heart Association, 2*(5), e000461. https://doi.org/10.1161/JAHA.113.000461

Dorn, G. W. (2015). Mitochondrial dynamism and heart disease: Changing shape and shaping change. *EMBO Molecular Medicine, 7*(7), 865–877. https://doi.org/10.15252/emmm.201404575

Du, C., Anderson, A., Lortie, M., Parsons, R., & Bodnar, A. (2013). Oxidative damage and cellular defense mechanisms in sea urchin models of aging. *Free Radical Biology & Medicine, 63,* 254–263. https://doi.org/10.1016/j.freeradbiomed.2013.05.023

Guo, Y., Koshy, S., Hui, D., Palmer, J. L., Shin, K., Bozkurt, M., & Wamique Yusuf, S. (2015). Prognostic value of heart rate variability in patients with cancer. *Journal of Clinical Neurophysiology, 32*(6), 516–520. https://doi.org/10.1097/WNP.0000000000000210

Guzzetti, S., Costantino, G., Vernocchi, A., Sada, S., & Fundarò, C. (2008). First diagnosis of colorectal or breast cancer and prevalence of atrial fibrillation. *Internal and Emergency Medicine, 3*(3), 227–231. https://doi.org/10.1007/s11739-008-0124-4

Hahn, W. S., Kuzmicic, J., Burrill, J. S., Donoghue, M. A., Foncea, R., Jensen, M. D., ... Bernlohr, D. A. (2014). Proinflammatory cytokines differentially regulate adipocyte mitochondrial metabolism, oxidative stress, and dynamics. *American Journal of Physiology-Endocrinology and*

Metabolism, 306(9), E1033–E1045. https://doi.org/10.1152/ajpendo.00422.2013

Hequet, O., Le, Q. H., Moullet, I., Pauli, E., Salles, G., Espinouse, D., … Coiffier, B. (2004). Subclinical late cardiomyopathy after doxorubicin therapy for lymphoma in adults. *Journal of Clinical Oncology: Official Journal of the American Society of Clinical Oncology, 22*(10), 1864–1871. https://doi.org/10.1200/JCO.2004.06.033

Ishida, J., Saitoh, M., Doehner, W., von Haehling, S., Anker, M., Anker, S. D., & Springer, J. (2017). Animal models of cachexia and sarcopenia in chronic illness: Cardiac function, body composition changes and therapeutic results. *International Journal of Cardiology, 238*, 12–18. https://doi.org/10.1016/j.ijcard.2017.03.154

Kim, J., Kundu, M., Viollet, B., & Guan, K.-L. (2011). AMPK and mTOR regulate autophagy through direct phosphorylation of Ulk1. *Nature Cell Biology, 13*(2), 132–141. https://doi.org/10.1038/ncb2152

Kirshenbaum, L. A. (2012). Regulation of autophagy in the heart in health and disease. *Journal of Cardiovascular Pharmacology, 60*(2), 109. https://doi.org/10.1097/FJC.0b013e31825f6faa

Kobayashi, S., Xu, X., Chen, K., & Liang, Q. (2012). Suppression of autophagy is protective in high glucose-induced cardiomyocyte injury. *Autophagy, 8*(4), 577–592. https://doi.org/10.4161/auto.18980

Koleini, N., & Kardami, E. (2017). Autophagy and mitophagy in the context of doxorubicin-induced cardiotoxicity. *Oncotarget, 8*(28), 46663–46680. https://doi.org/10.18632/oncotarget.16944

Kuzmicic, J., del Campo, A., López-Crisosto, C., Morales, P. E., Pennanen, C., Bravo-Sagua, R., … Lavandero, S. (2011). Dinámica mitocondrial: Un potencial nuevo blanco terapéutico para la insuficiencia cardiaca. *Revista española de cardiología, 64*(10), 916–923. https://doi.org/10.1016/j.recesp.2011.05.018

Lainscak, M., Dagres, N., Filippatos, G. S., Anker, S. D., & Kremastinos, D. T. (2008). Atrial fibrillation in chronic non-cardiac disease: Where do we stand? *International Journal of Cardiology, 128*(3), 311–315. https://doi.org/10.1016/j.ijcard.2007.12.078

Lavandero, S., Troncoso, R., Rothermel, B. A., Martinet, W., Sadoshima, J., & Hill, J. A. (2013). Cardiovascular autophagy. *Autophagy, 9*(10), 1455–1466. https://doi.org/10.4161/auto.25969

Li, D. L., Wang, Z. V., Ding, G., Tan, W., Luo, X., Criollo, A., … Hill, J. A. (2016). Doxorubicin blocks cardiomyocyte autophagic flux by inhibiting lysosome acidification. *Circulation, 133*(17), 1668–1687. https://doi.org/10.1161/CIRCULATIONAHA.115.017443

Li, S., Wang, W., Niu, T., Wang, H., Li, B., Shao, L., … Cui, T. (2014). Nrf2 deficiency exaggerates doxorubicin-induced cardiotoxicity and cardiac dysfunction. *Oxidative Medicine and Cellular Longevity, 2014*, 748524. https://doi.org/10.1155/2014/748524

Mann, D. L. (2002). Inflammatory mediators and the failing heart: Past, present, and the foreseeable future. *Circulation Research, 91*(11), 988–998. Retrieved from. http://www.ncbi.nlm.nih.gov/pubmed/12456484

Marano, G., Vergari, A., Catalano, L., Gaudi, S., Palazzesi, S., Musumeci, M., … Ferrari, A. U. (2004). Na⁺/H⁺ exchange inhibition attenuates left ventricular remodeling and preserves systolic function in pressure-overloaded hearts. *British Journal of Pharmacology, 141*(3), 526–532. https://doi.org/10.1038/sj.bjp.0705631

Matarrese, P., Abbruzzese, C., Mileo, A. M., Vona, R., Ascione, B., Visca, P., … Paggi, M. G. (2016). Interaction between the human papillomavirus 16 E7 oncoprotein and gelsolin ignites cancer cell motility and invasiveness. *Oncotarget, 7*(32), 50972–50985. https://doi.org/10.18632/oncotarget.8646

Matarrese, P., Tinari, A., Mormone, E., Bianco, G. A., Toscano, M. A., Ascione, B., … Malorni, W. (2005). Galectin-1 sensitizes resting human T lymphocytes to Fas (CD95)-mediated cell death via mitochondrial hyperpolarization, budding, and fission. *Journal of Biological Chemistry, 280*(8), 6969–6985. https://doi.org/10.1074/jbc.M409752200

McGrath, J., Drummond, G., McLachlan, E., Kilkenny, C., & Wainwright, C. (2010). Guidelines for reporting experiments involving animals: The ARRIVE guidelines. *British Journal of Pharmacology, 160*(7), 1573–1576. https://doi.org/10.1111/j.1476-5381.2010.00873.x

McGrath, J. C., & Lilley, E. (2015). Implementing guidelines on reporting research using animals (ARRIVE etc.): New requirements for publication in BJP. *British Journal of Pharmacology, 172*(13), 3189–3193. https://doi.org/10.1111/bph.12955

Mejia, E. M., Cole, L. K., & Hatch, G. M. (2014). Cardiolipin metabolism and the role it plays in heart failure and mitochondrial supercomplex formation. *Cardiovascular & Hematological Disorders Drug Targets, 14*(2), 98–106. Retrieved from. http://www.ncbi.nlm.nih.gov/pubmed/24801725

Minotti, G., Menna, P., Salvatorelli, E., Cairo, G., & Gianni, L. (2004). Anthracyclines: Molecular advances and pharmacologic developments in antitumor activity and cardiotoxicity. *Pharmacological Reviews, 56*(2), 185–229. https://doi.org/10.1124/pr.56.2.6

Moulin, M., Piquereau, J., Mateo, P., Fortin, D., Rucker-Martin, C., Gressette, M., … Ventura-Clapier, R. (2015). Sexual dimorphism of doxorubicin-mediated cardiotoxicity. *Circulation: Heart Failure, 8*(1), 98–108. https://doi.org/10.1161/CIRCHEARTFAILURE.114.001180

Moulin, M., Solgadi, A., Veksler, V., Garnier, A., Ventura-Clapier, R., & Chaminade, P. (2015). Sex-specific cardiac cardiolipin remodelling after doxorubicin treatment. *Biology of Sex Differences, 6*(1), 20. https://doi.org/10.1186/s13293-015-0039-5

Nakai, A., Yamaguchi, O., Takeda, T., Higuchi, Y., Hikoso, S., Taniike, M., … Otsu, K. (2007). The role of autophagy in cardiomyocytes in the basal state and in response to hemodynamic stress. *Nature Medicine, 13*(5), 619–624. https://doi.org/10.1038/nm1574

Octavia, Y., Tocchetti, C. G., Gabrielson, K. L., Janssens, S., Crijns, H. J., & Moens, A. L. (2012). Doxorubicin-induced cardiomyopathy: From molecular mechanisms to therapeutic strategies. *Journal of Molecular and Cellular Cardiology, 52*(6), 1213–1225. https://doi.org/10.1016/j.yjmcc.2012.03.006

Ong, S.-B., Kalkhoran, S. B., Cabrera-Fuentes, H. A., & Hausenloy, D. J. (2015). Mitochondrial fusion and fission proteins as novel therapeutic targets for treating cardiovascular disease. *European Journal of Pharmacology, 763*(Pt A), 104–114. https://doi.org/10.1016/j.ejphar.2015.04.056

Patrizio, M., Musumeci, M., Stati, T., Fasanaro, P., Palazzesi, S., Catalano, L., & Marano, G. (2007). Propranolol causes a paradoxical enhancement of cardiomyocyte foetal gene response to hypertrophic stimuli. *British Journal of Pharmacology, 152*(2), 216–222. https://doi.org/10.1038/sj.bjp.0707350

Pizarro, M., Troncoso, R., Martínez, G. J., Chiong, M., Castro, P. F., & Lavandero, S. (2016). Basal autophagy protects cardiomyocytes from doxorubicin-induced toxicity. *Toxicology, 370*, 41–48. https://doi.org/10.1016/j.tox.2016.09.011

Sciarretta, S., Maejima, Y., Zablocki, D., & Sadoshima, J. (2018). The role of autophagy in the heart. *Annual Review of Physiology, 80*(1), 1–26. https://doi.org/10.1146/annurev-physiol-021317-121427

Seviiri, M., Lynch, B. M., Hodge, A. M., Yang, Y., Liew, D., English, D. R., & Dugué, P. A. (2018). Resting heart rate, temporal changes in resting heart rate, and overall and cause-specific mortality. *Heart*, 1076–1085. https://doi.org/10.1136/heartjnl-2017-312251

Shenouda, S. M., Widlansky, M. E., Chen, K., Xu, G., Holbrook, M., Tabit, C. E., … Vita, J. A. (2011). Altered mitochondrial dynamics contributes to endothelial dysfunction in diabetes mellitus. *Circulation, 124*(4), 444–453. https://doi.org/10.1161/CIRCULATIONAHA.110.014506

Štěrba, M., Popelová, O., Vávrová, A., Jirkovský, E., Kovaříková, P., Geršl, V., & Šimůnek, T. (2013). Oxidative stress, redox signaling, and metal chelation in anthracycline cardiotoxicity and pharmacological cardioprotection. *Antioxidants & Redox Signaling, 18*(8), 899–929. https://doi.org/10.1089/ars.2012.4795

Tilemann, L. M., Heckmann, M. B., Katus, H. A., Lehmann, L. H., & Müller, O. J. (2018). Cardio-oncology: Conflicting priorities of

anticancer treatment and cardiovascular outcome. *Clinical Research in Cardiology, 107*(4), 271–280. https://doi.org/10.1007/s00392-018-1202-x

Tran, S., DeGiovanni, P.-J., Piel, B., & Rai, P. (2017). Cancer nanomedicine: A review of recent success in drug delivery. *Clinical and Translational Medicine, 6*(1), 44. https://doi.org/10.1186/s40169-017-0175-0

Ventura-Clapier, R., Garnier, A., Veksler, V., & Joubert, F. (2011). Bioenergetics of the failing heart. *Biochimica et Biophysica Acta (BBA) - Molecular Cell Research, 1813*(7), 1360–1372. https://doi.org/10.1016/J.BBAMCR.2010.09.006

Yoon, Y., Krueger, E. W., Oswald, B. J., & McNiven, M. A. (2003). The mitochondrial protein hFis1 regulates mitochondrial fission in mammalian cells through an interaction with the dynamin-like protein DLP1. *Molecular and Cellular Biology, 23*(15), 5409–5420. Retrieved from. http://www.ncbi.nlm.nih.gov/pubmed/12861026

Yu, T., Jhun, B. S., & Yoon, Y. (2011). High-glucose stimulation increases reactive oxygen species production through the calcium and mitogen-activated protein kinase-mediated activation of mitochondrial fission. *Antioxidants & Redox Signaling, 14*(3), 425–437. https://doi.org/10.1089/ars.2010.3284

Zhao, X., Zhang, W., Xing, D., Li, P., Fu, J., Gong, K., ... Chen, Y.-F. (2013). Endothelial cells overexpressing IL-8 receptor reduce cardiac remodeling and dysfunction following myocardial infarction. *American Journal of Physiology Heart and Circulatory Physiology, 305*(4), H590–H598. https://doi.org/10.1152/ajpheart.00571.2012

SUPPORTING INFORMATION

Additional supporting information may be found online in the Supporting Information section at the end of the article.